Supplementary materials
for

Tumor-associated macrophages contribute to cisplatin resistance via regulating Pol η-mediated translesion DNA synthesis in ovarian cancer

Bilash Chatterjee[1,2], Mrinmoy Sarkar[1], Debanjana Ghosh[1], Sangita Mishra[1], Subhankar Bose[1,2] , Md. Maqsood Ahamad Khan[3,] , Senthil Kumar Ganesan[3], Nabanita Chatterjee[4], Amit Kumar Srivastava[1,2*]

[1]Cancer Biology and Inflammatory Disorder Division, CSIR-Indian Institute of Chemical Biology, Kolkata, West Bengal, India.
[2]Academy of Scientific and Innovative Research (AcSIR), Ghaziabad, Uttar Pradesh, India 201002.
[3]Structural Biology and Bioinformatics Division, CSIR-Indian Institute of Chemical Biology, Kolkata, West Bengal, India.
[4]Chittaranjan National Cancer Institute (CNCI), Kolkata, West Bengal, India.

*Corresponding author
Email id. - amit@iicb.res.in

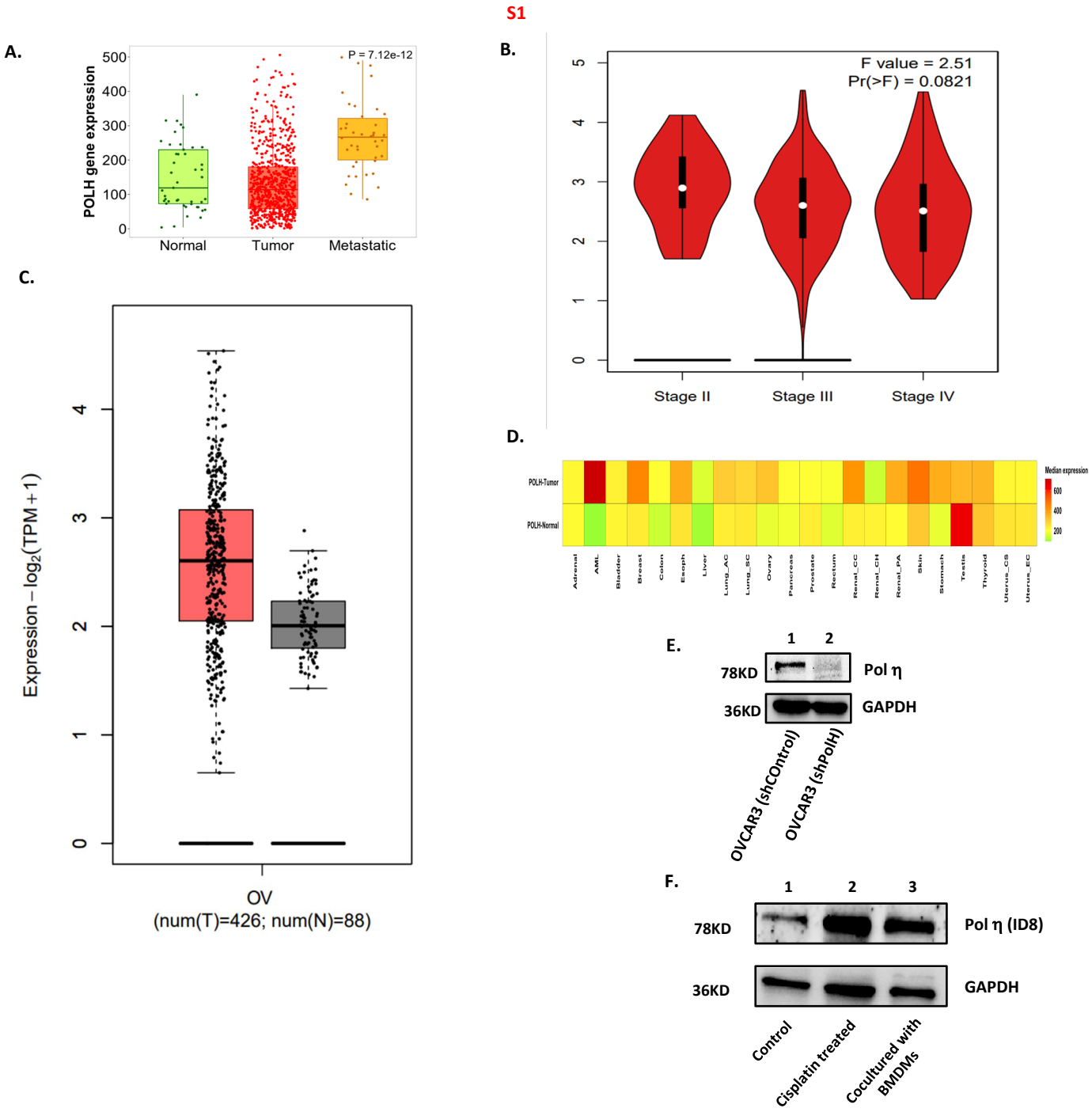

Fig. S1 (**A, B**) Clinical relevance of Pol η expression in terms of cancer stages and aggressiveness of ovarian cancer (from TCGA database). **(C.)** Differential level of transcripts per million in normal vs tumor tissues for Pol η **(D.)** Heatmap showing the Pan cancer differential expression of Pol η in normal vs tumor tissue (TNMplot) (**E.**) Confirmation of Pol η expression level in OVCAR3 (shControl) and OVCAR3 (shPOLH) cells through western blot analysis. GAPDH was used as the loading control. **(F.)** Western blot analysis of Pol η expression in mice ID8 cell line cocultured with mice bone marrow-derived primary macrophages. GAPDH was used as the loading control.

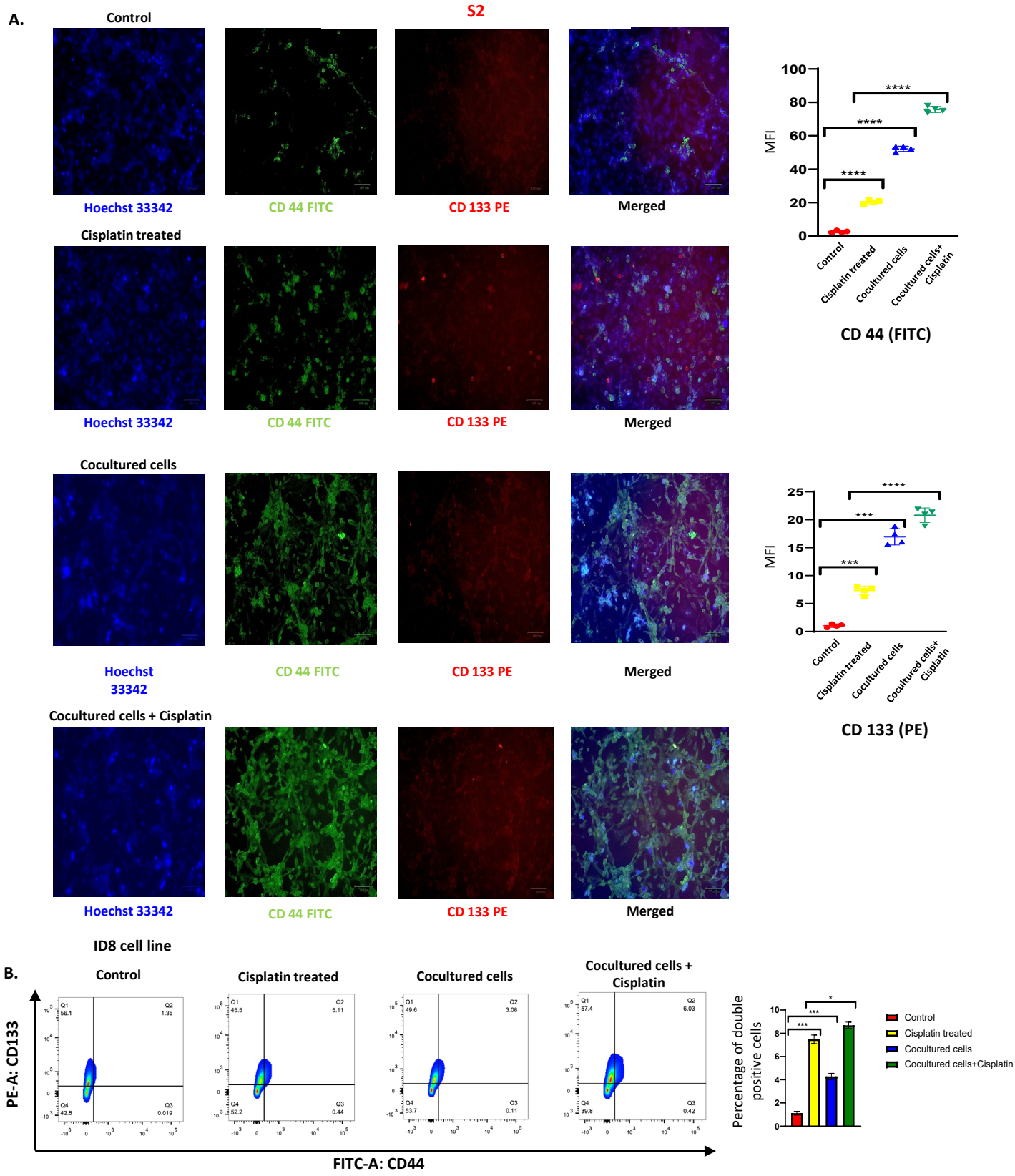

Fig. S2. (**A.**) Live ID8 mouse ovarian cells were immunostained to assess differential expression of stemness markers CD44 and CD133 using FITC- and PE-conjugated antibodies, respectively, across various treatment groups. Nuclei were counterstained with Hoechst 33342. Fluorescence microscopy images were captured from triplicate experiments. Quantification of fluorescence intensity is shown as mean ± SD. ***p<0.001, ****p<0.0001. (**B.**) Flow cytometry analysis of the ID8 cell line was performed to identify the $CD44^{+}CD133^{+}$ double-positive cancer stem-like cell population. Experiments were conducted in triplicate, and the percentage of this population is presented as mean ± SD. For panel A and B, Brown-Forsythe ANOVA test followed by Games-Howell's multiple comparisons test was performed, where, *p<0.05, ****p<0.0001.

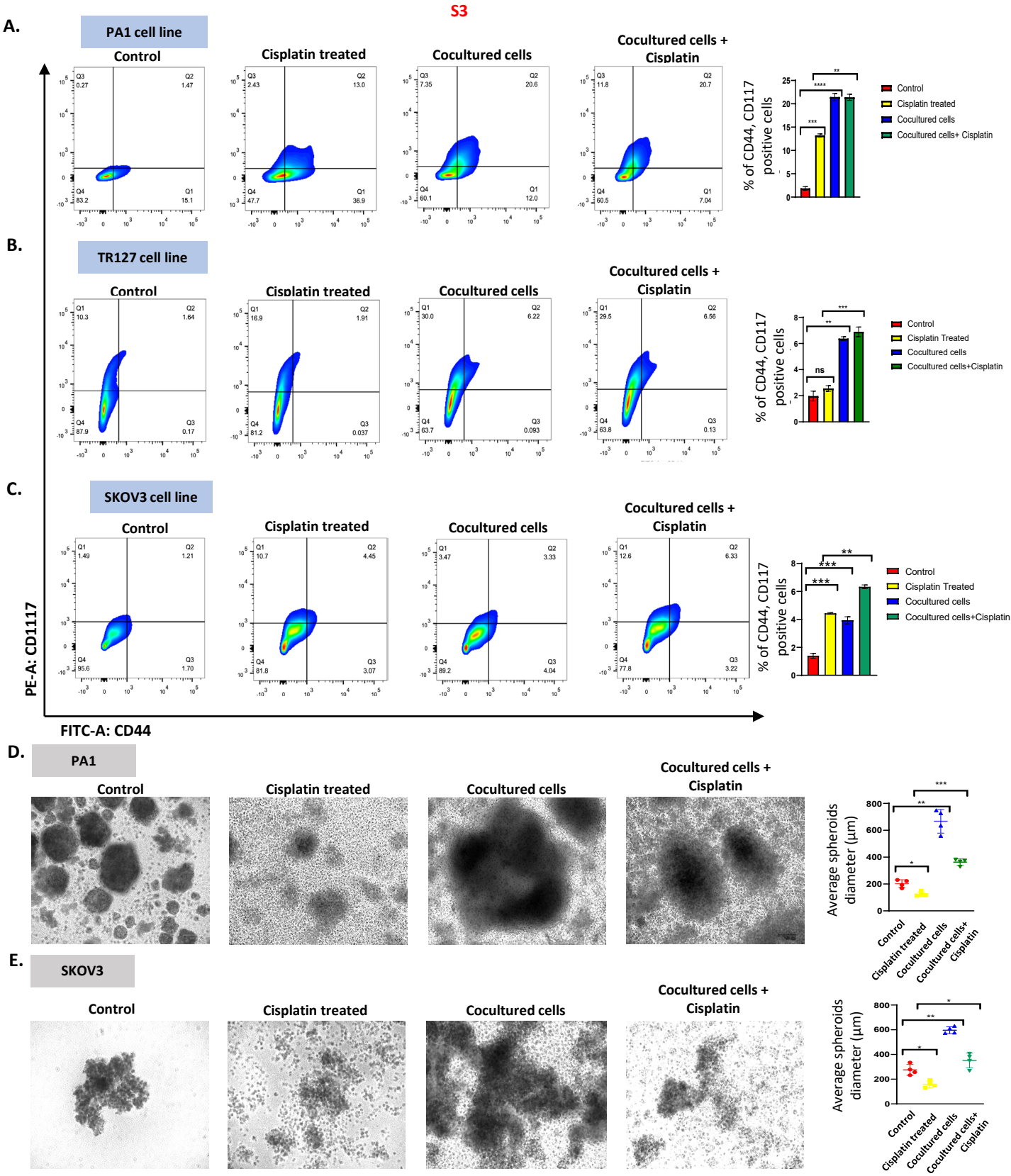

Fig. S3 (A, B, C) Three cell lines PA1, TR127 (cisplatin-resistant), and SKOV3 were seeded separately. The cells were subsequently collected and processed for flow cytometry analysis to analyze the population of $CD44^{+}CD117^{+}$ double-positive cancer stem-like cells. All the flow cytometry-based experiments were performed in triplicates and graphically represented as mean ± SD, *p<0.05, **p<0.01, ***p<0.001, ****p<0.0001. **(D, E)** PA1 and SKOV3 cell lines were seeded in an ultra-low attachment culture dish in cancer stem cell media (0.2×10^{6} cells/dish). Spheroids were allowed to grow for 72 hours to determine the average cancer cell spheroids' diameter**.** The experiments were repeated in triplicates and pictures were taken under a brightfield inverted microscope. The average spheroid diameter is graphically depicted as mean ± SD, scale bar=100µm. For all the figure panels, the Brown-Forsythe ANOVA test followed by Games-Howell's multiple comparisons test was performed, *p<0.05, **p<0.01, ***p<0.001.

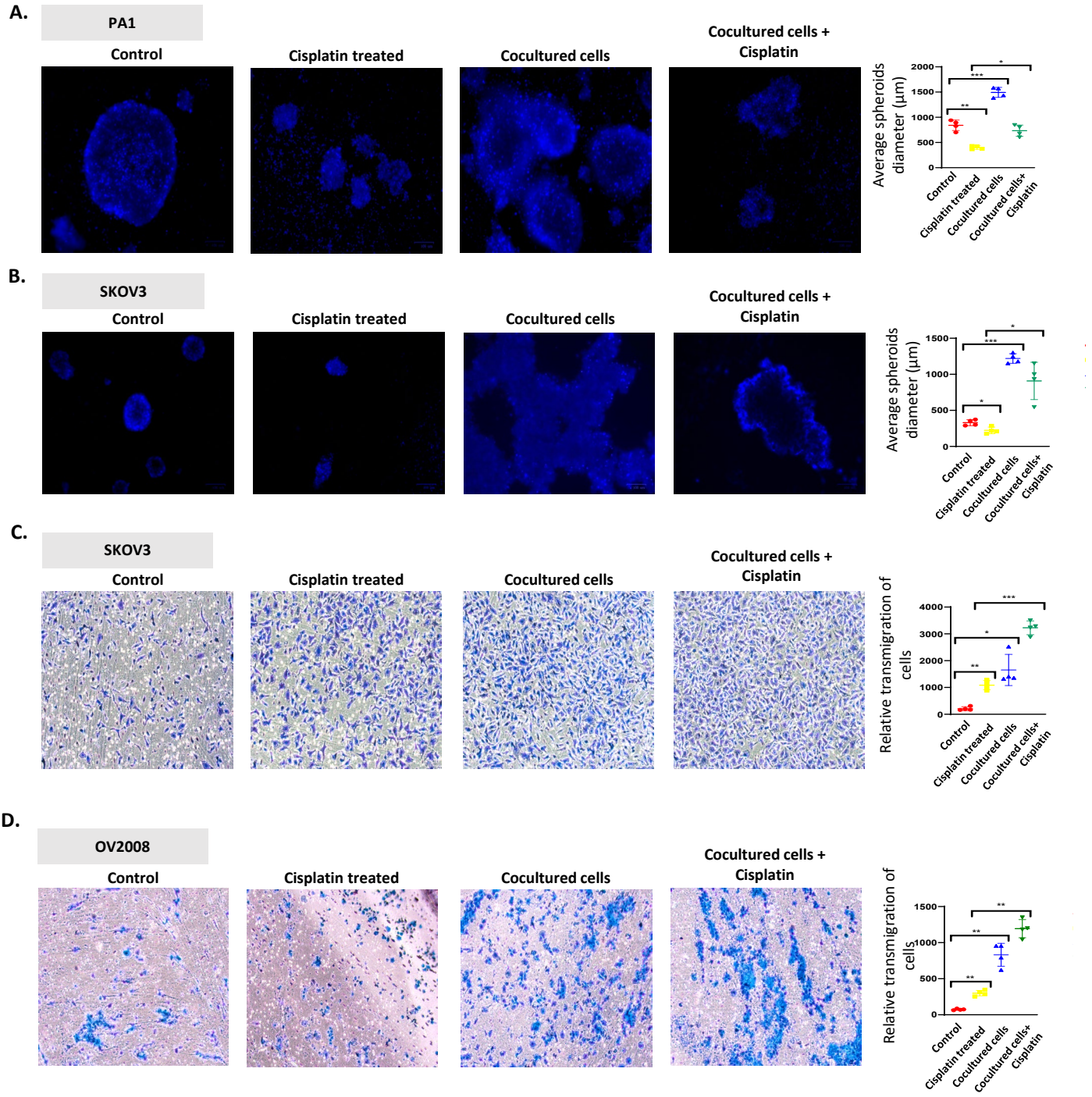

Fig. S4 (A, B) A total of 0.2 × 10^6 PA1 and SKOV3 cells were seeded in ultralow attachment plates and cultured for 72 hours to allow spheroid formation. Live cells within the spheroids were stained with Hoechst 33342 dye and visualized by fluorescence microscopy. The average spheroid diameter is presented as mean ± SD.. *p<0.05, **p<0.01, ***p<0.001, Scale bar=100µm. **(C, D)** Around 30,000 cells (SKOV3 and OV2008) cells were seeded for trans-well migration assay. Experimental data is represented as the mean ± SD of three replicates of the assay where, **p<0.01, ***p<0.001, ****p<0.0001. For all the figure panels, the Brown-Forsythe ANOVA test followed by Games-Howell's multiple comparisons test was performed.

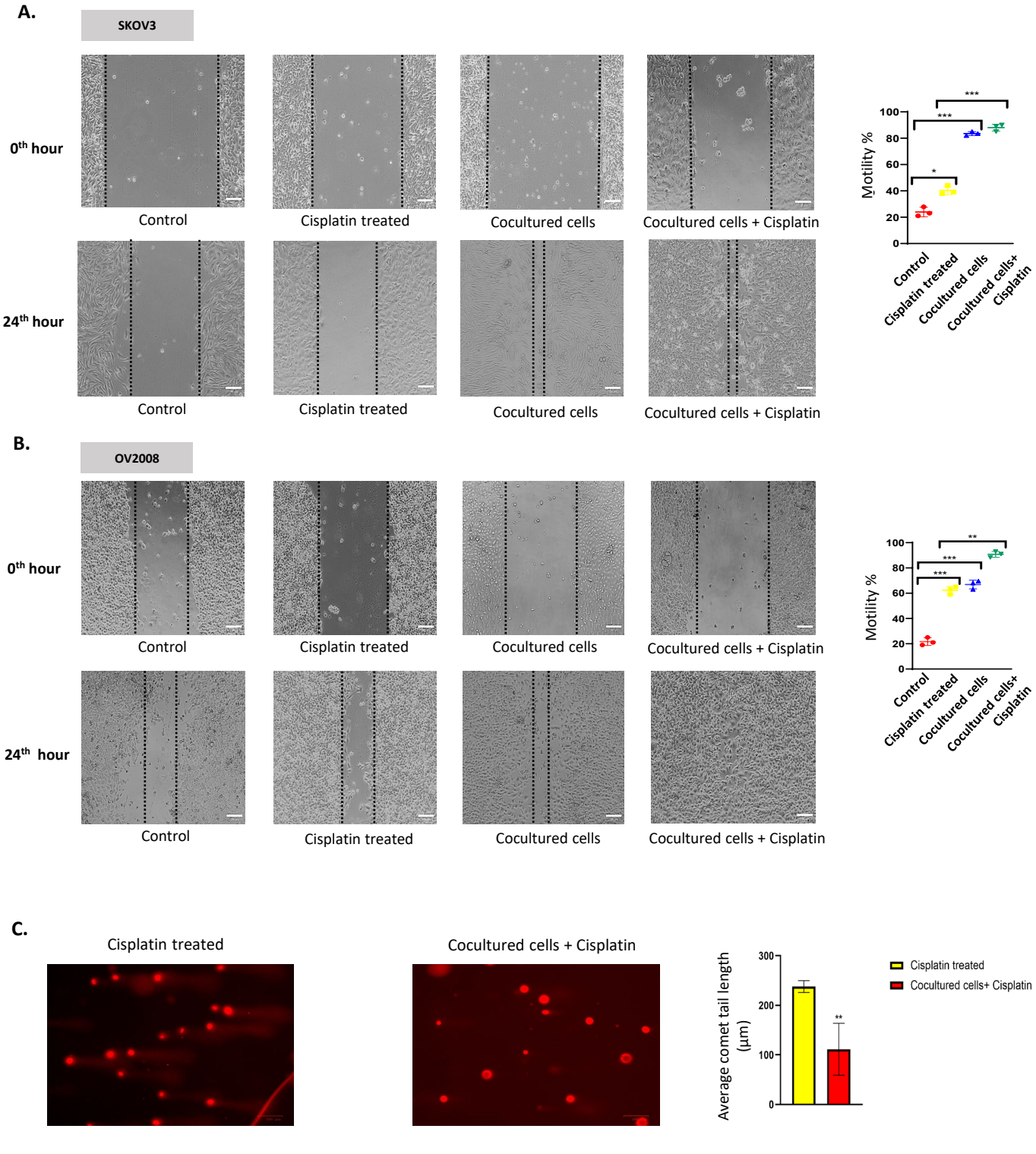

Fig. S5 (A, B) OV2008 and SKOV3 cells were seeded in six-well plates for the wound healing assay. The experiment was performed in triplicate, and cell motility percentage is presented as mean ± SD.. **p<0.01, ***p<0.001, ****p<0.0001. Scale bar=100µm. **(C.)** Comet tail length differences in OV2008 cells were quantified by comet assay and displayed as mean ± SD on a bar graph from three independent experiments. **p<0.01. Scale bar=100µm. For panels, A and B, the Brown-Forsythe ANOVA test followed by Games-Howell's multiple comparisons test was performed. For panel C, an unpaired student's t-test was performed.

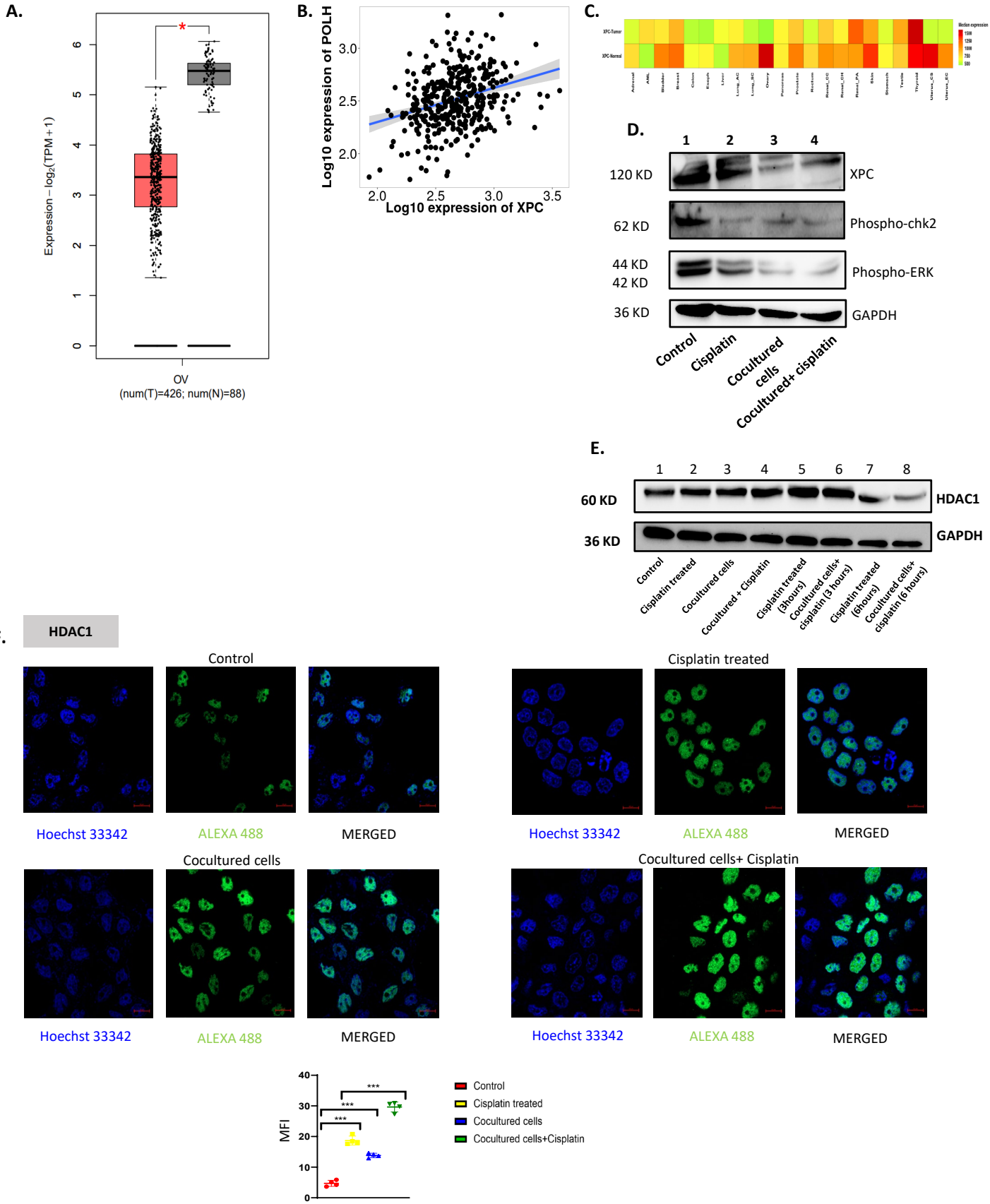

Fig. S6 (A.) Differential level of transcripts per million in normal and tumor tissues for *XPC* gene in ovarian tissue. **(B.)** Expression correlation of *XPC* and *POLH* in clinical samples. **(C.)** Heatmap showing the PAN Cancer differential expression of *XPC* in normal vs tumor tissue. **(D, E.)** Proteins were extracted from the OVCAR3 cell line for western blot analysis of HDAC1, Phospho-ERK1/2, Phospho-CHK2, and XPC among the experimental groups. GAPDH was used as the loading control. **(F.)** OV2008 cells were seeded on coverslips and subjected to immunocytochemistry to assess nuclear localization of HDAC1 across experimental groups. Fluorescence intensity was quantified and presented as mean ± SD from three independent experiments. Scale bar=20µm, *p<0.05. For panel C, the Brown-Forsythe ANOVA test followed by Games-Howell's multiple comparisons test was performed.

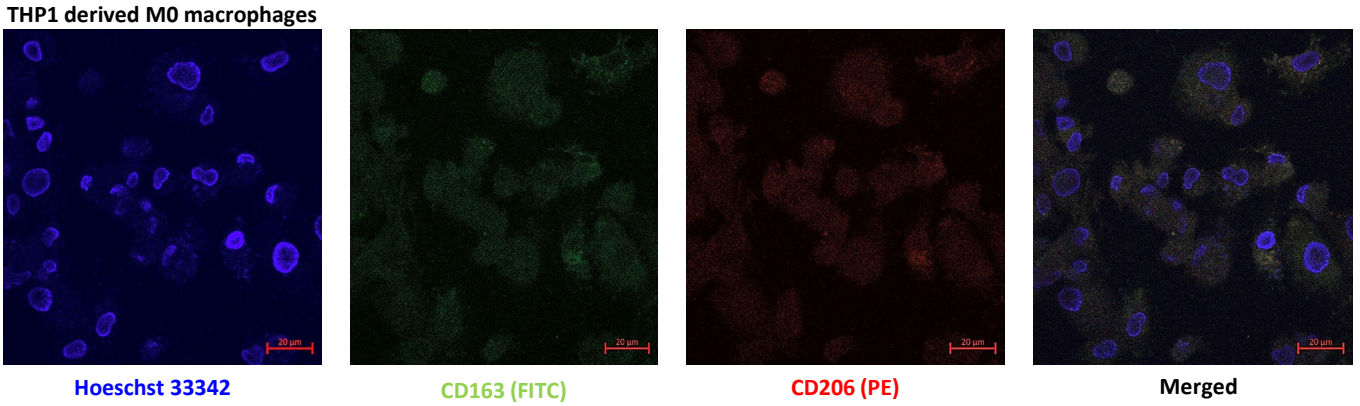

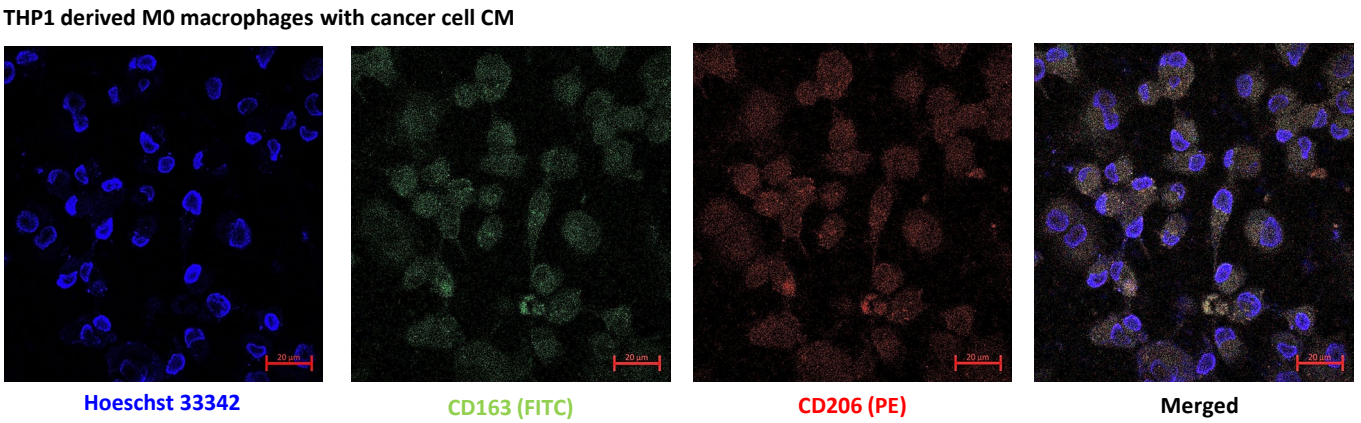

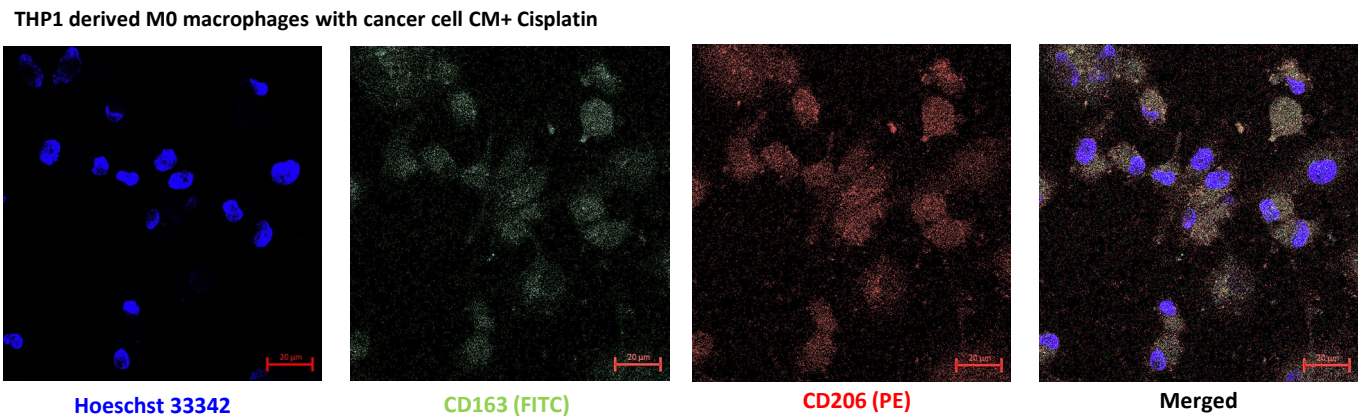

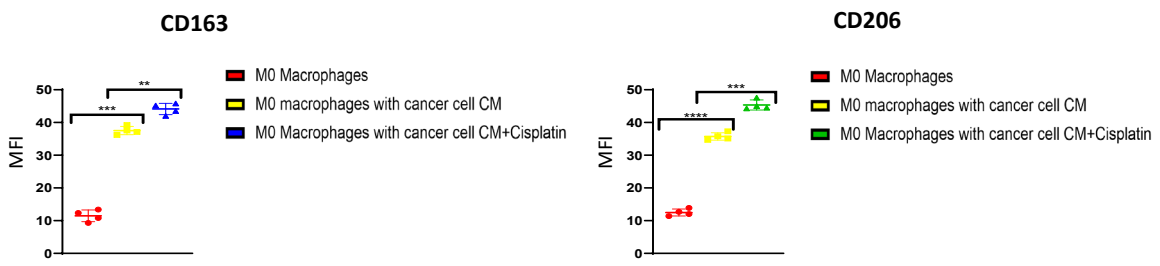

Fig. S7. Immunocytochemistry analysis of $CD163^{+}CD206^{+}$ double-positive M2-like macrophages differentiated from PMA-treated THP-1 cells seeded on coverslips. Cells were imaged using a confocal microscope with a 63× objective, and fluorescence intensity was quantified and presented as mean ± SD from three independent experiments. Scale bar= 20µm, *p<0.05, **p<0.01, ***p<0.001, ****p<0.0001. For all the figure panels, the Brown-Forsythe ANOVA test followed by Games-Howell's multiple comparisons test was performed.

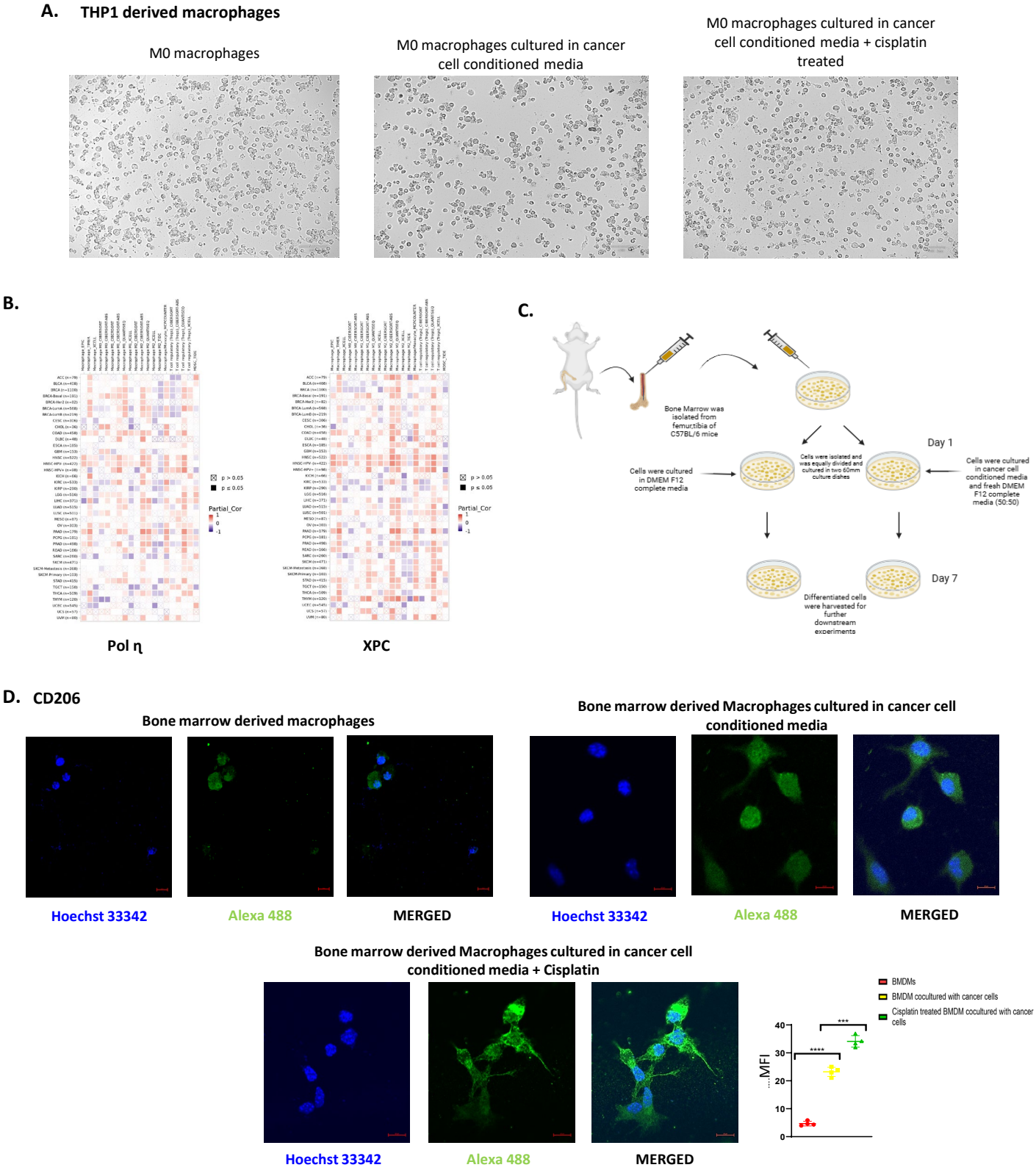

Fig. S8 (A.) Brightfield microscopic images of THP-1-derived M0 macrophages, cultured with or without ovarian cancer cell-conditioned media, followed by cisplatin treatment. Scale bar = 100 µm. **(B.)** Heatmap depicting the PAN Cancer correlation between *POLH* and *XPC* expression and immune cell sub-population infiltration in tumors. **(C.)** Diagrammatic representation of the isolation and culturing of bone marrow-derived primary macrophages from C57BL/6 mice. **(D.)** Confocal microscopy images of CD206-immunostained THP-1-derived macrophages captured using a 100× objective. Mean fluorescence intensity is presented as mean ± SD from three independent experiments. Scale bar 10µm. ***p<0.001, ****p<0.0001. For panel D, the Brown-Forsythe ANOVA test followed by Games-Howell's multiple comparisons test was performed.

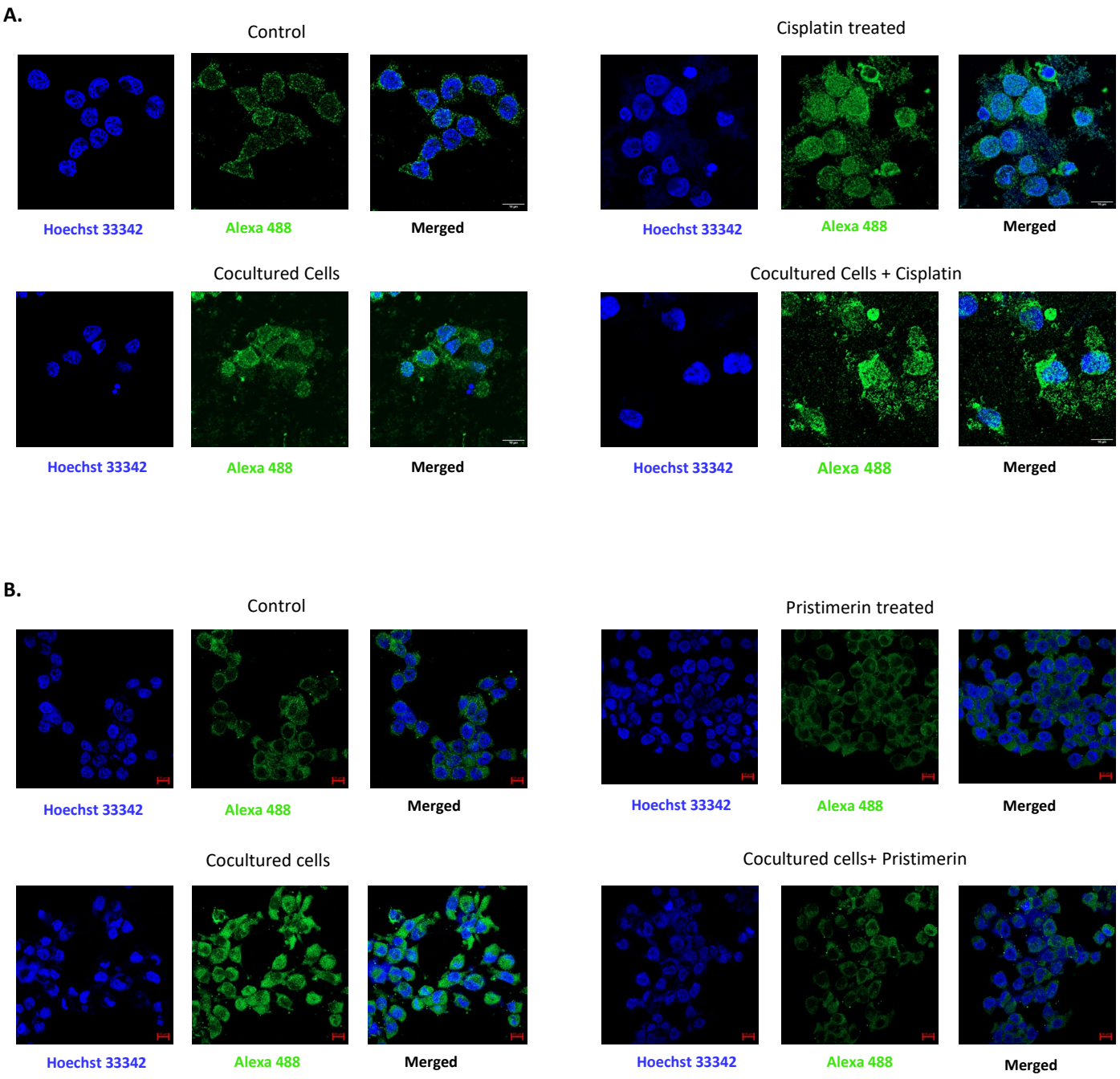

Fig. S9 (A) Confocal microscopy images from immunocytochemistry show the nuclear translocation of the p65 protein across different groups. OV2008 cells were seeded on coverslips, stained with a p65 primary antibody, and detected using an Alexa Fluor 488-conjugated anti-rabbit secondary antibody. **(B)** Immunocytochemistry analysis showing pristimerin-mediated inhibition of p65 nuclear translocation. OV2008 cells were seeded on coverslips, stained with a p65 primary antibody, and detected using an Alexa Fluor 488-conjugated anti-rabbit secondary antibody.

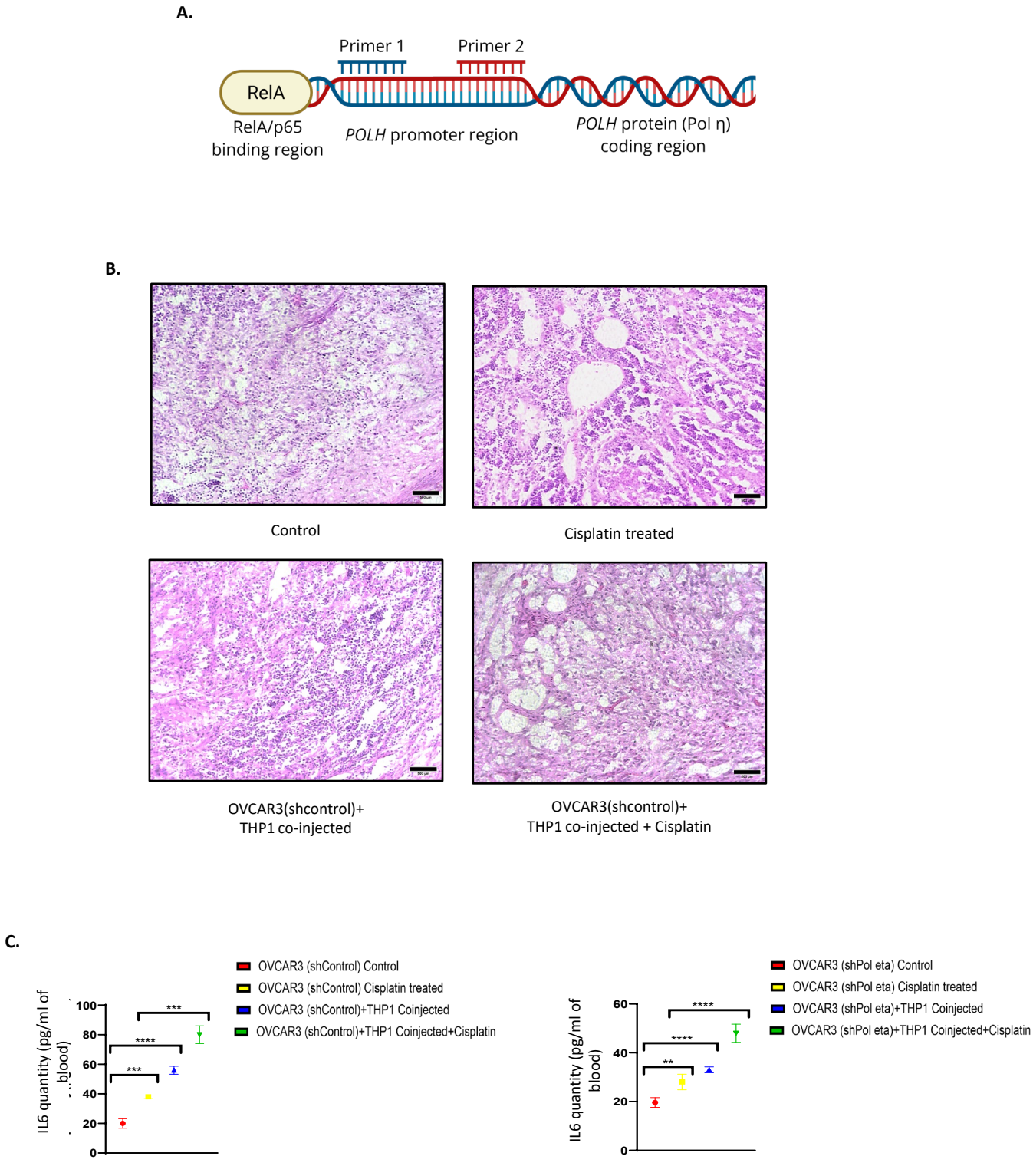

Fig. S10. (A) Schematic representation of primer design targeting the promoter region of *POLH* (Pol η). **(B)** Representative Hematoxylin and Eosin (H&E)-stained images of xenograft tumor tissue sections, showing histological changes. Images were captured using a brightfield microscope. Scale bar = 500 µm. **(C)** Graphical representation of IL-6 levels in mouse blood from the *in vivo* experiment across different experimental groups. **p<0.01, ****p<0.0001. For panel D, the Brown-Forsythe ANOVA test, followed by Games-Howell's multiple comparisons test, was performed.

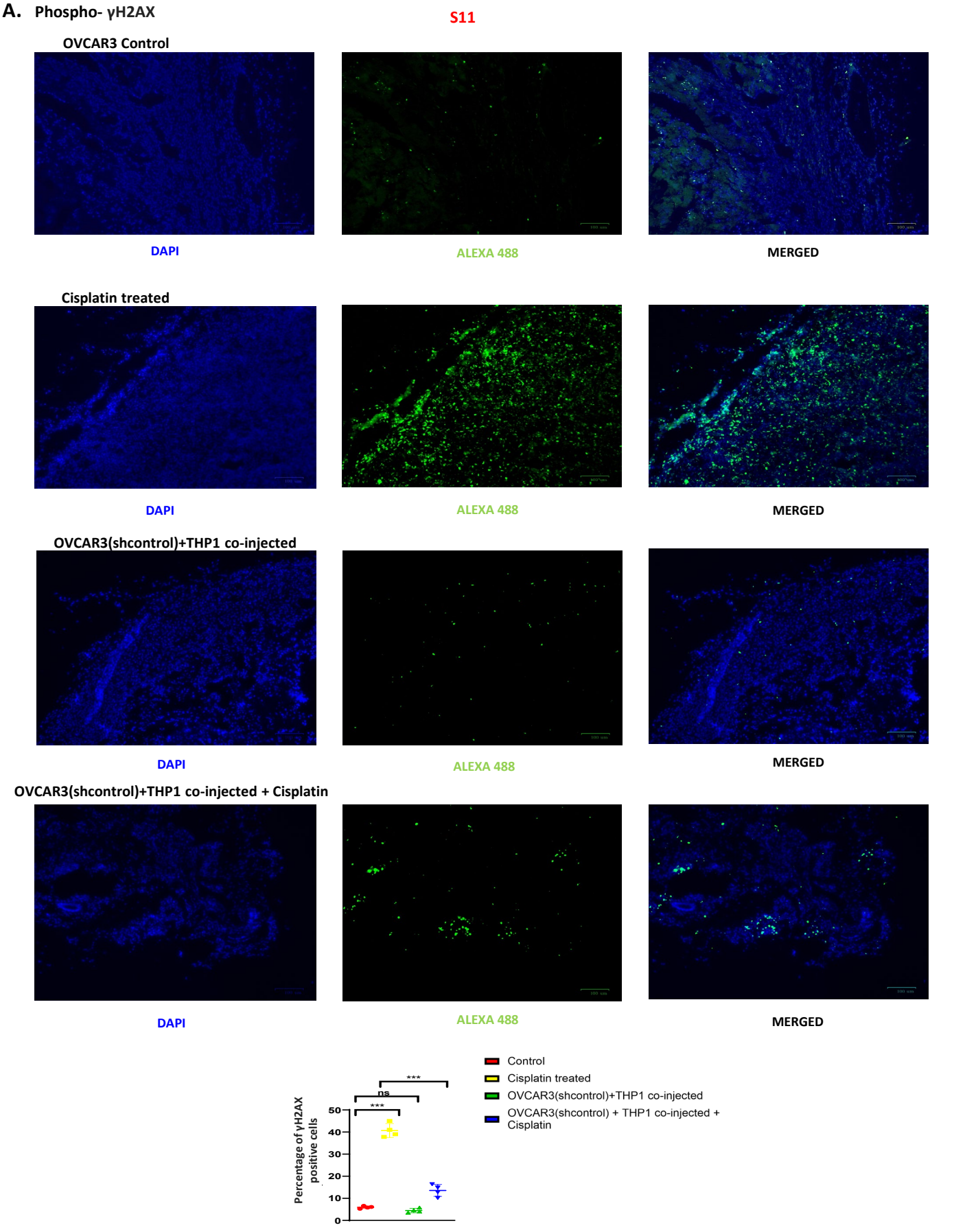

Fig. S11. Immunofluorescence staining of xenograft tumor tissue sections was performed using a phospho-γH2AX primary antibody, followed by detection with an Alexa Fluor 488-conjugated anti-rabbit secondary antibody. The percentage of phospho-γH2AX-positive cells is presented as mean ± SD from three independent experiments. *p<0.05, ***p<0.001.

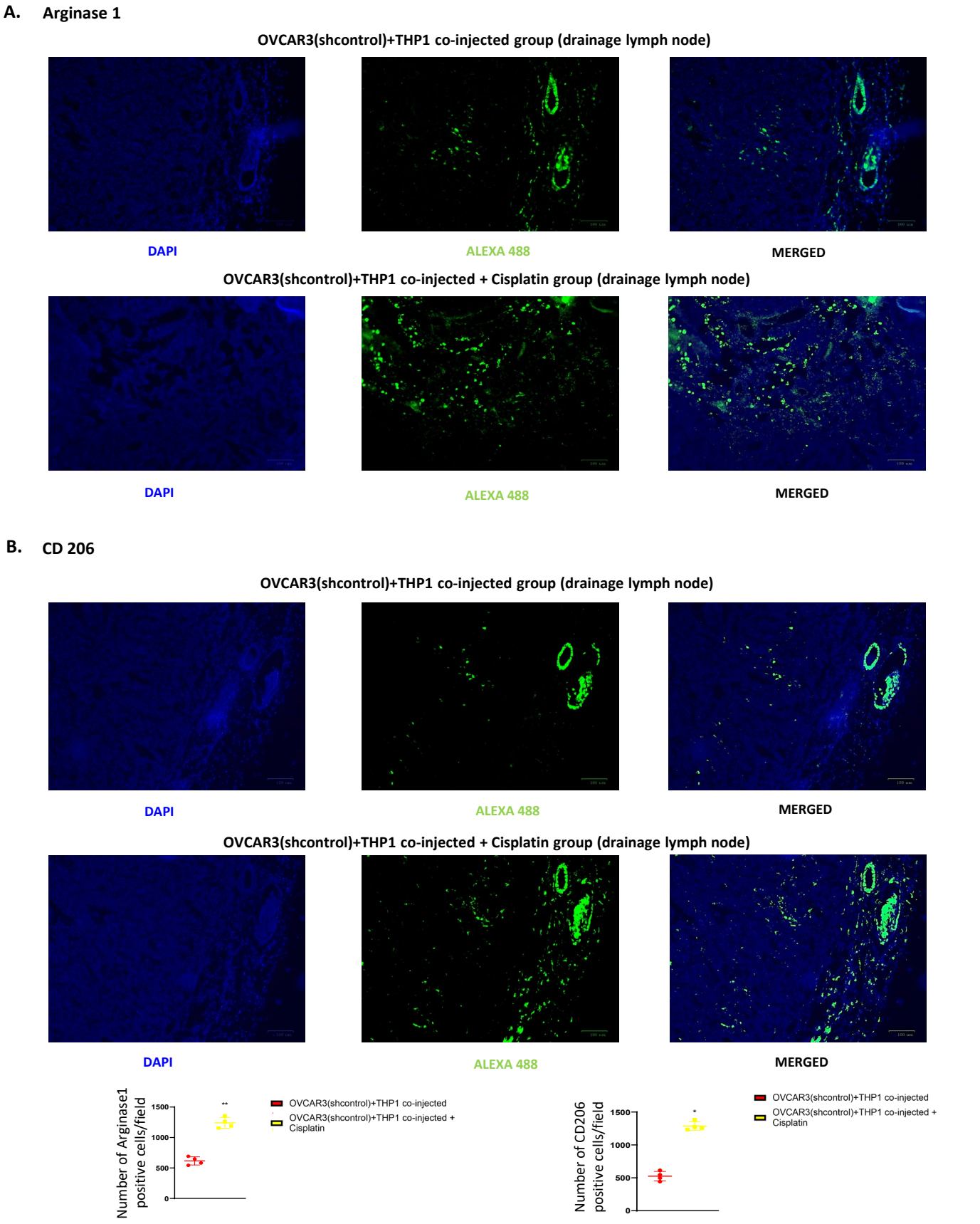

Fig. S12. Immunofluorescence staining was performed on inguinal lymph node tissue sections from mice in the xenograft tumor model. Sections were stained with human-specific Arginase-1 and CD206 primary antibodies, followed by detection with an Alexa Fluor 488-conjugated anti-rabbit secondary antibody. The number of Arginase-1$^+$ and CD206$^+$ cells per microscopic field is presented as mean ± SD from multiple tissue sections. *p<0.05, **p<0.01.

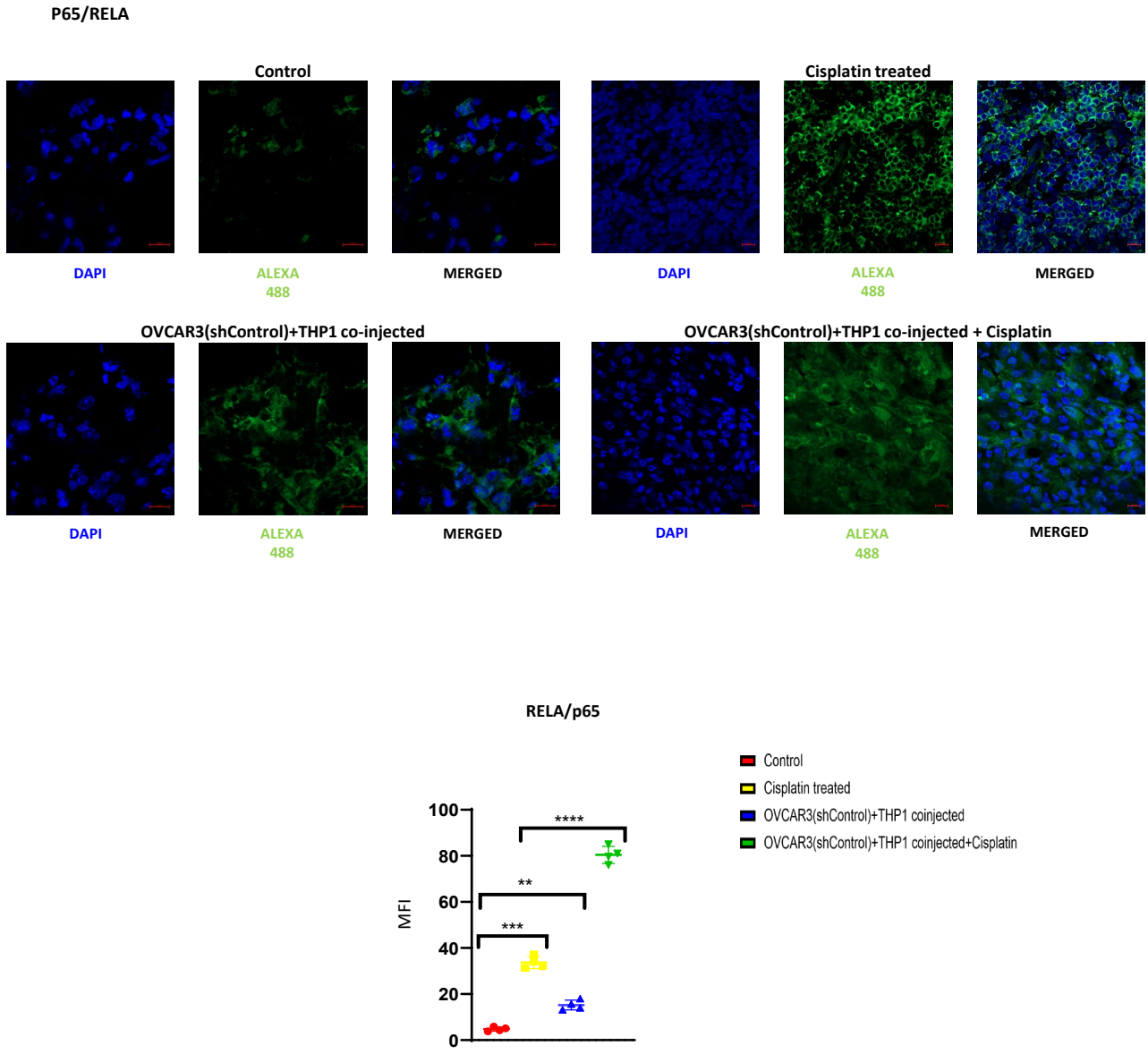

Fig. S13. Immunofluorescence staining of xenograft tumor tissue sections was performed using a p65 primary antibody. Images were captured using a confocal microscope with a 63× objective, and mean fluorescence intensity (MFI) is presented as mean ± SD from three independent experiments. Scale bar=10μm, *p<0.1, **p<0.01.

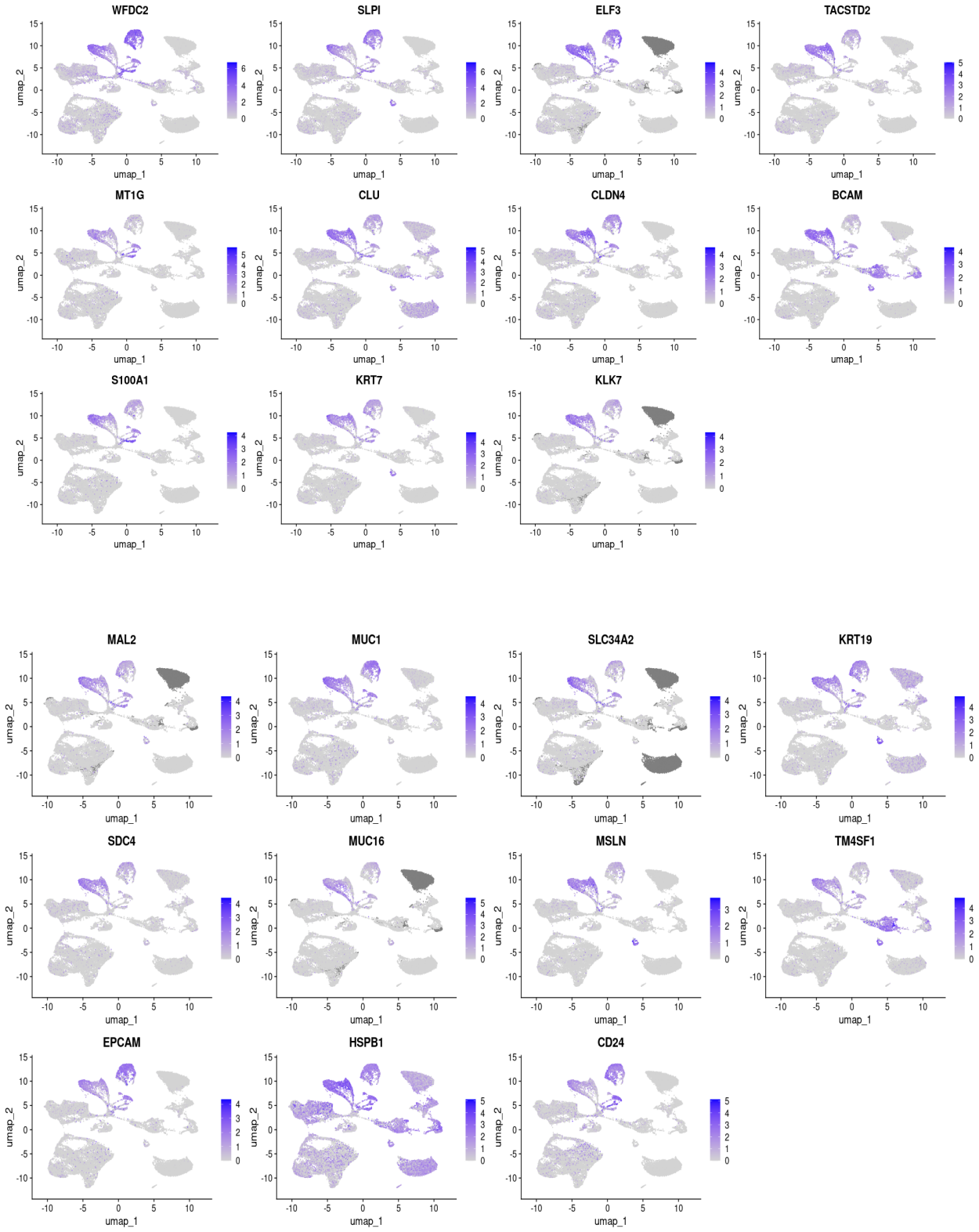

Fig. S14. The UMAP plots depict single-cell transcriptional profiles of representative genes associated with cancer cell clusters.

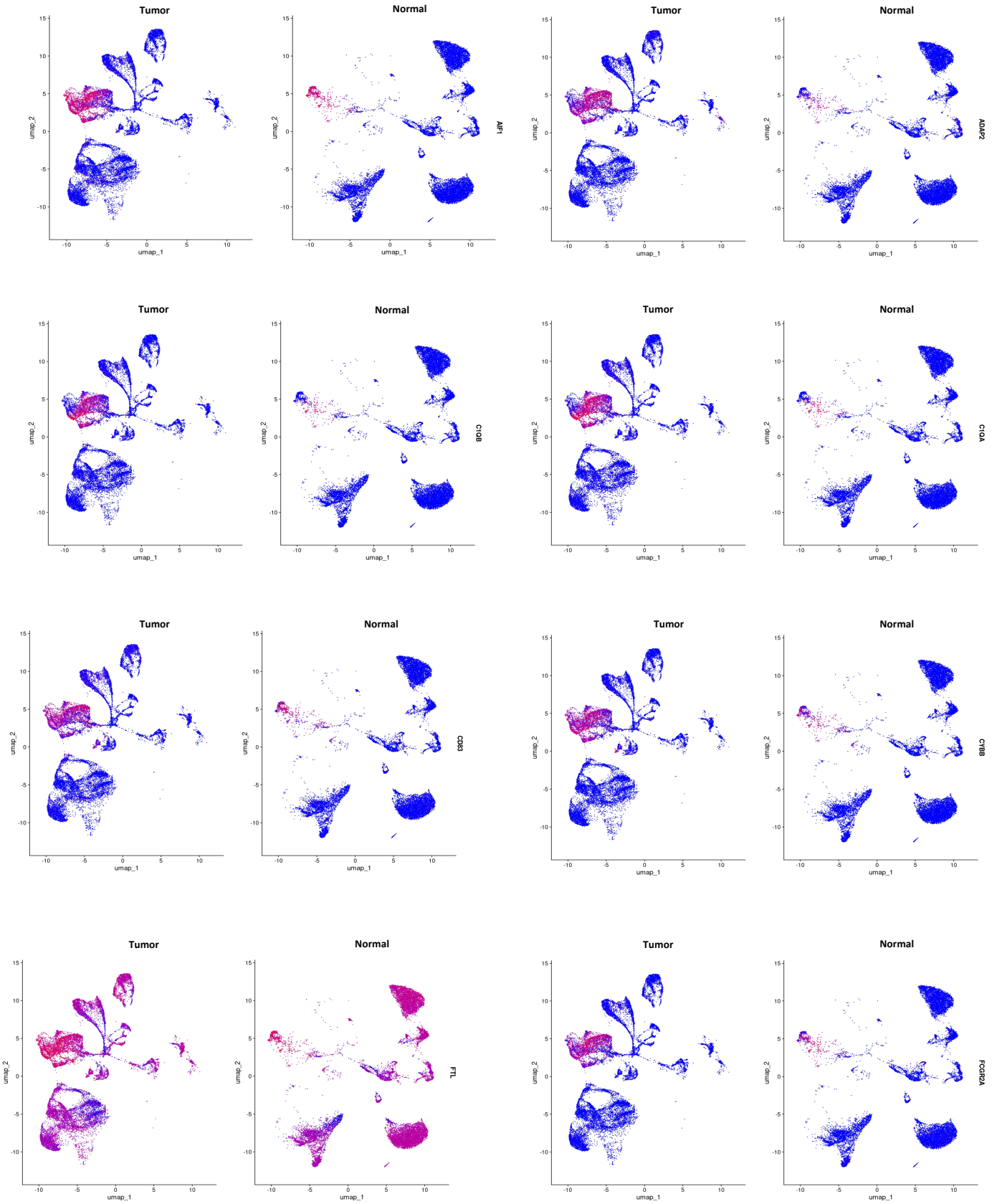

Fig. S15: The UMAP plots illustrate the differential single-cell transcriptional levels of representative genes in cancer cell clusters compared to normal cells.

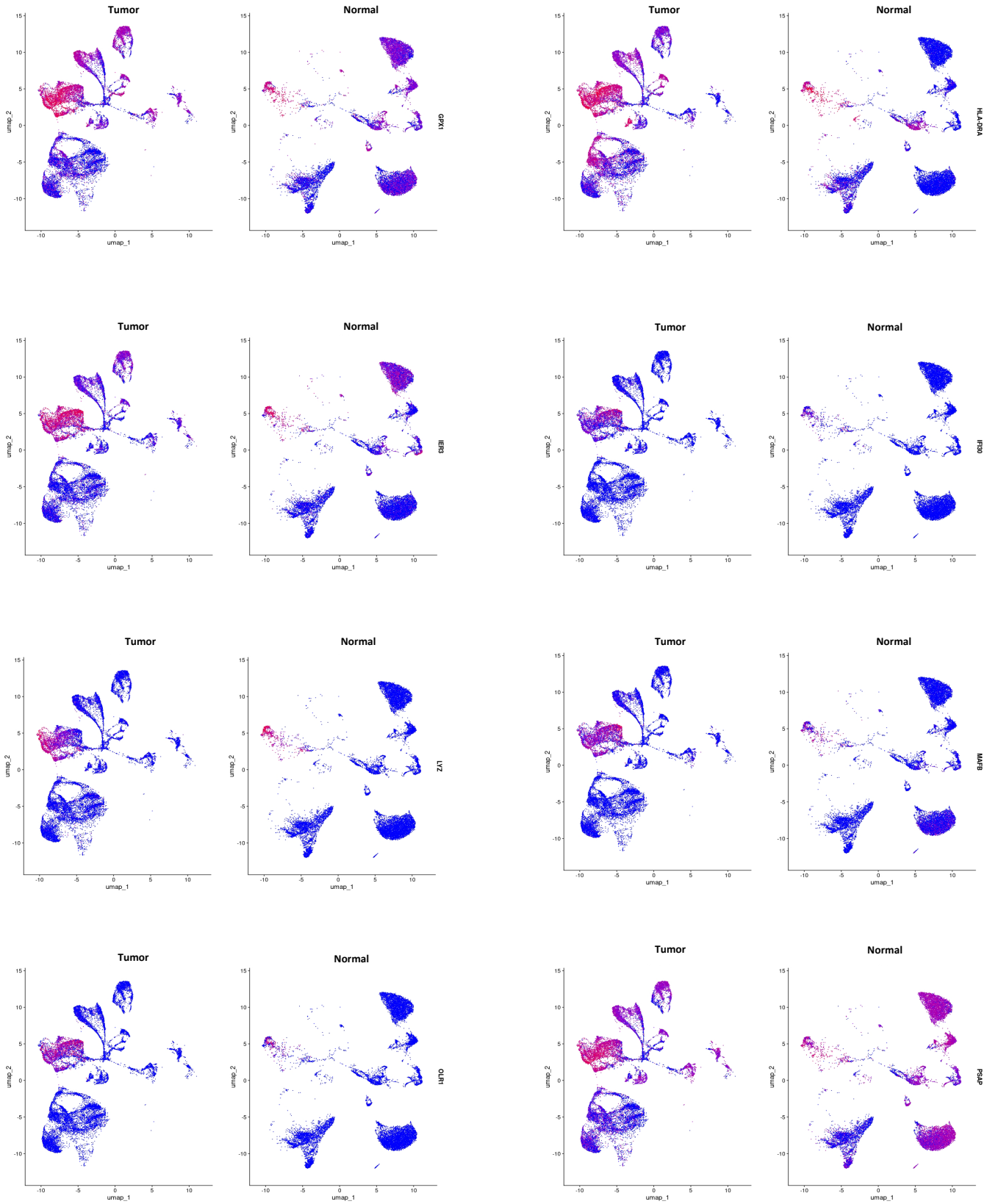

Fig. S16: The UMAP plots illustrate the differential single-cell transcriptional levels of representative genes in cancer cell clusters compared to normal cells.

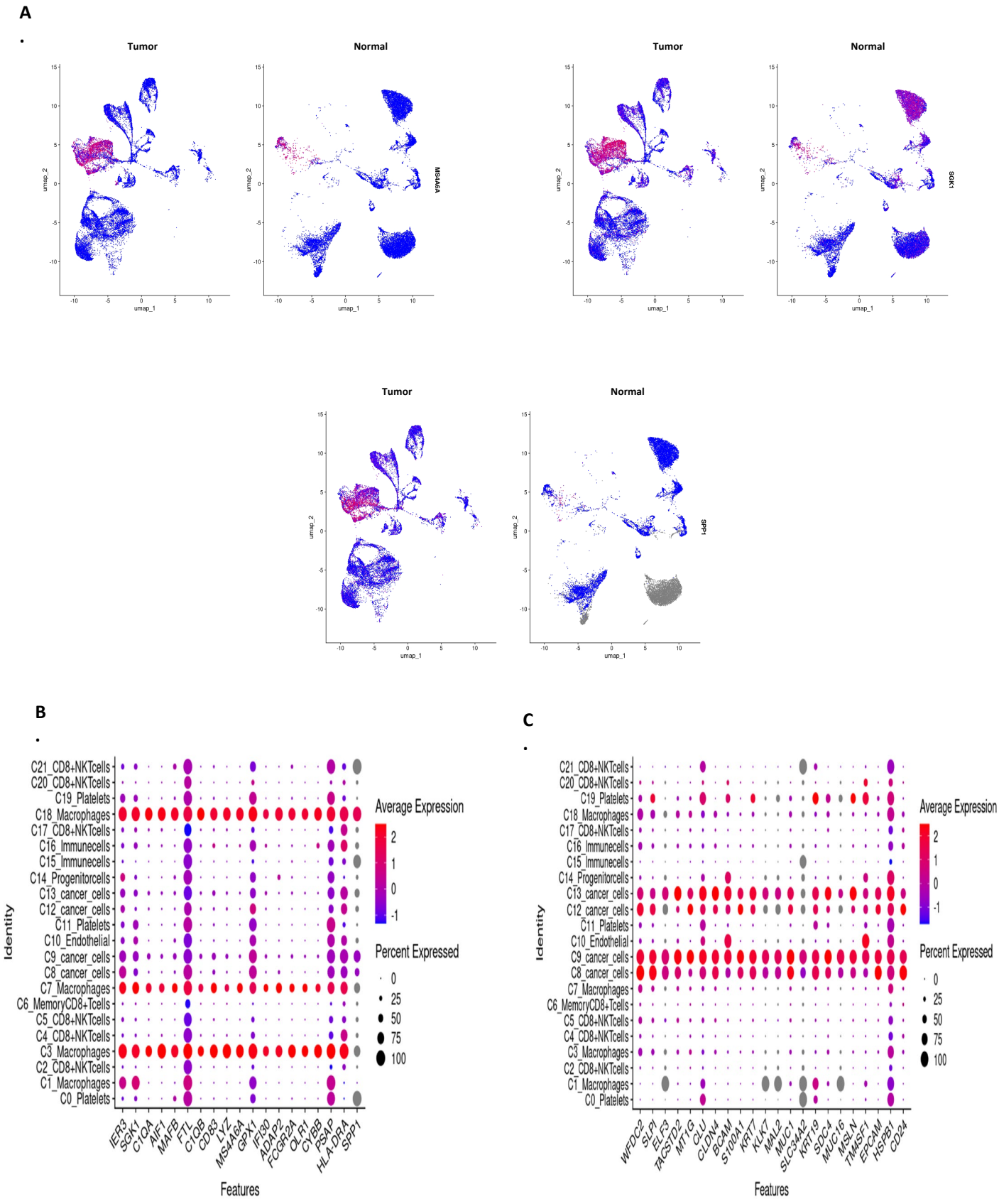

Fig. S17 (A) The UMAP plots illustrate the differential single-cell transcriptional levels of representative genes in cancer cell clusters compared to normal cells. (**B, C**) Dot plots show the transcriptional levels of representative genes across the identified single-cell clusters.

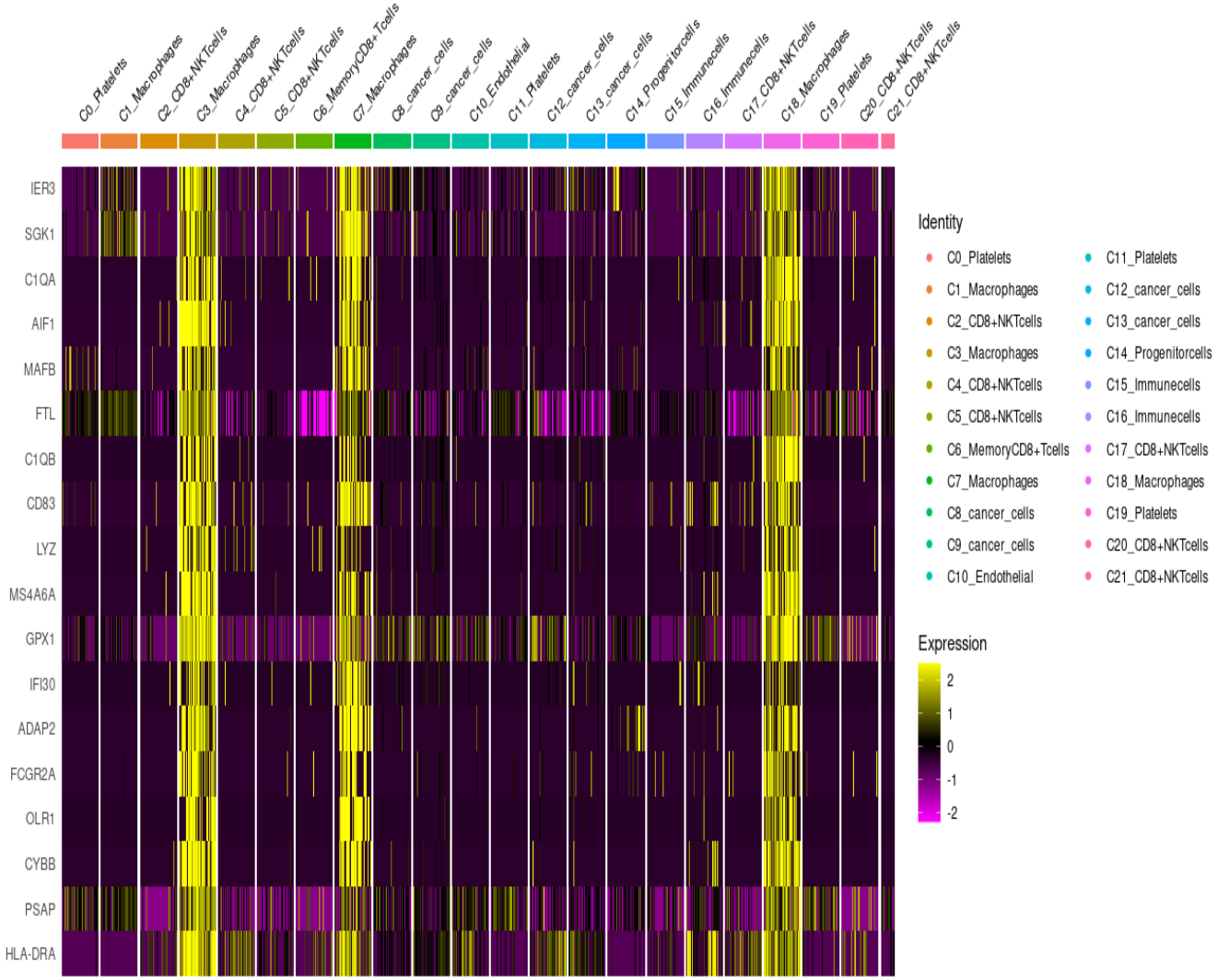

Fig. S18. Heatmap showing the differential expression (log_2 fold change) of representative genes across all identified cell clusters.

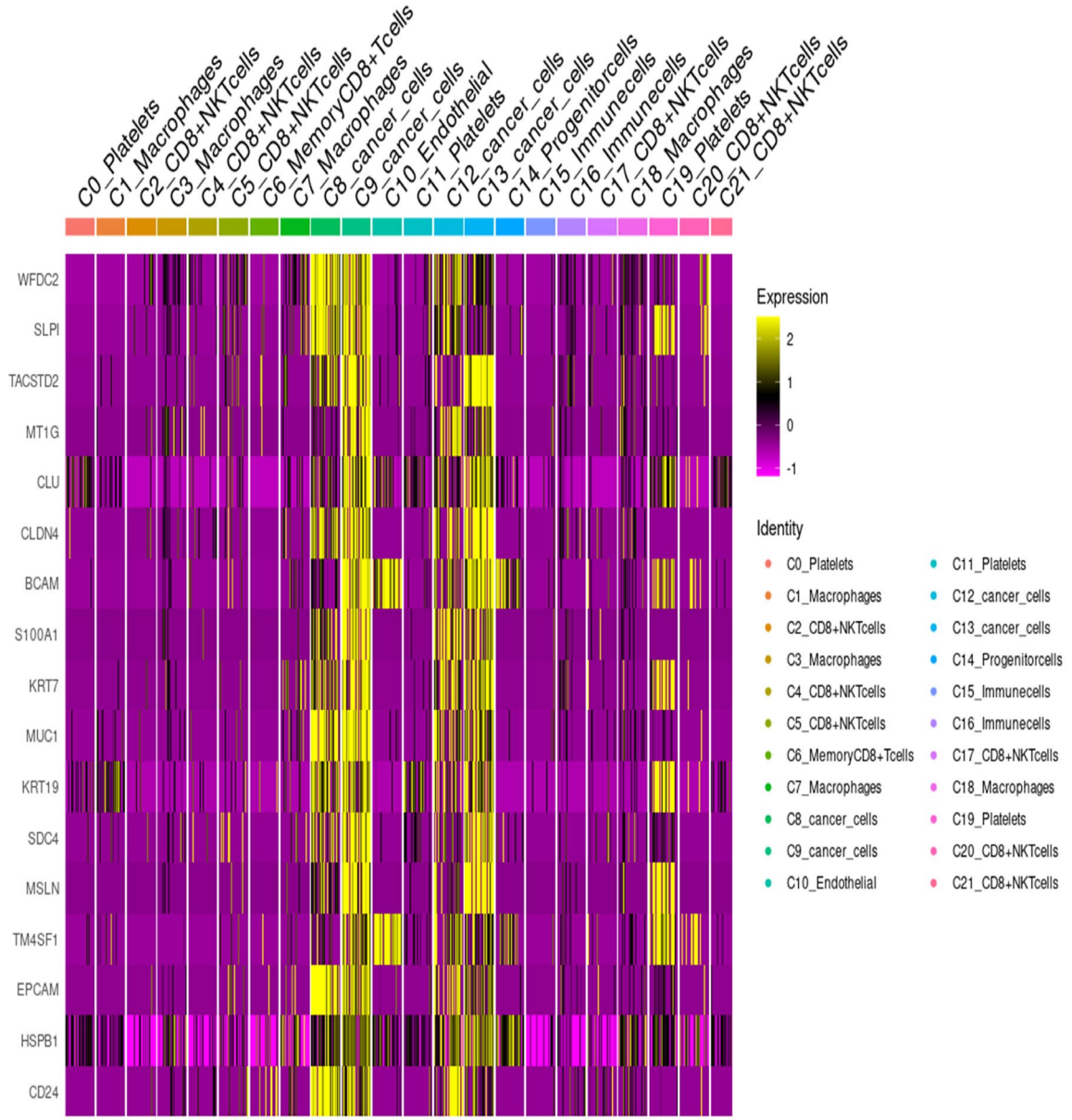

Fig. S19. Heatmap displays the $\log_2$ fold changes in expression levels of representative genes across the identified cell clusters.

A.

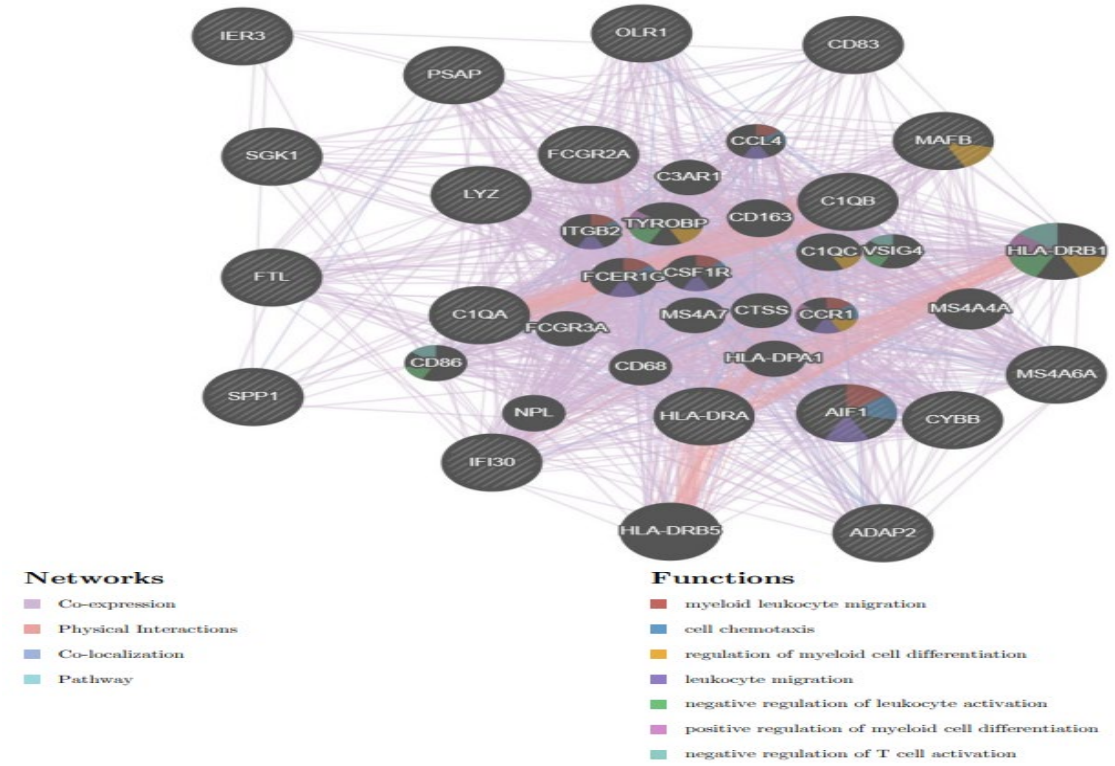

B.

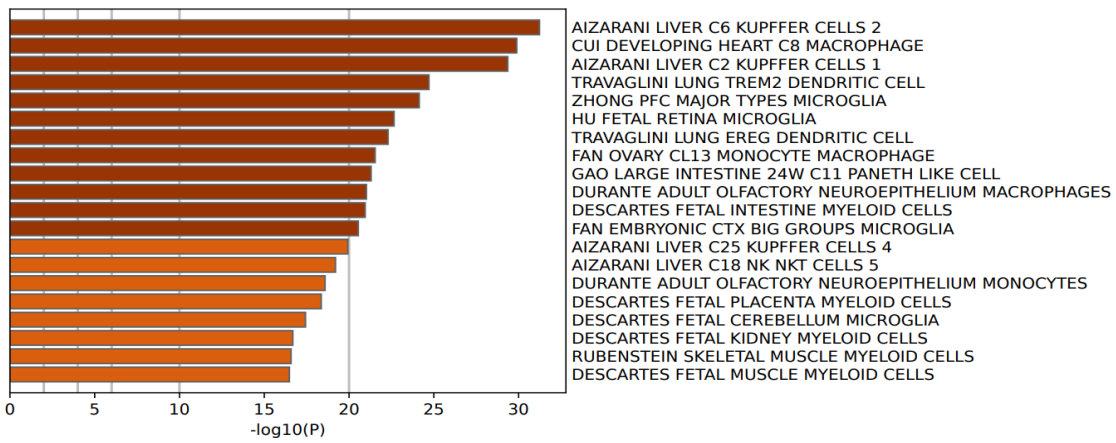

Fig. S20. (A) A protein–protein interaction (PPI) network was generated using representative genes from the identified macrophage clusters via the GeneMANIA web server. **(B)** Pathway enrichment analysis of representative genes from the cancer cell clusters was performed using the MetaScape web server.

A.

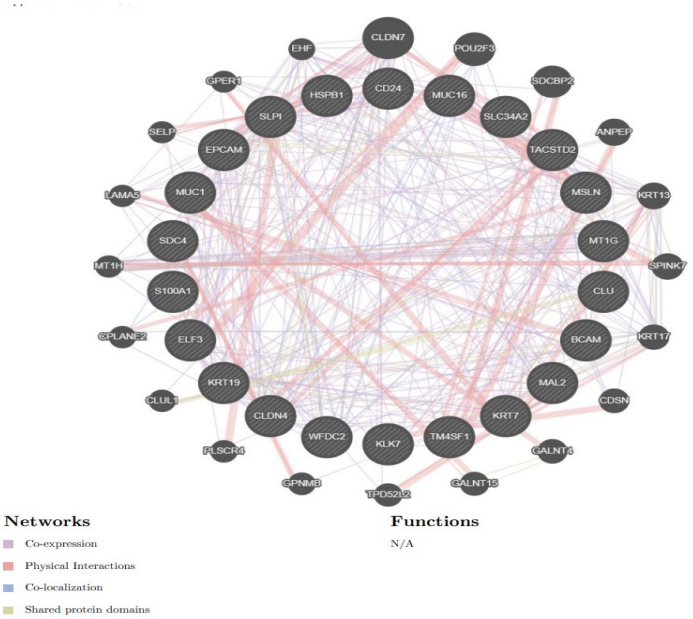

B.

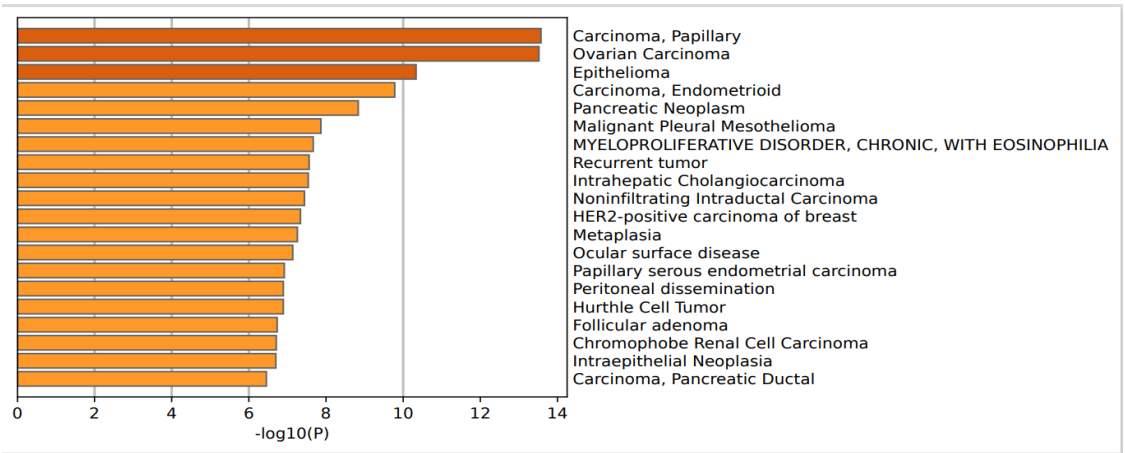

C.

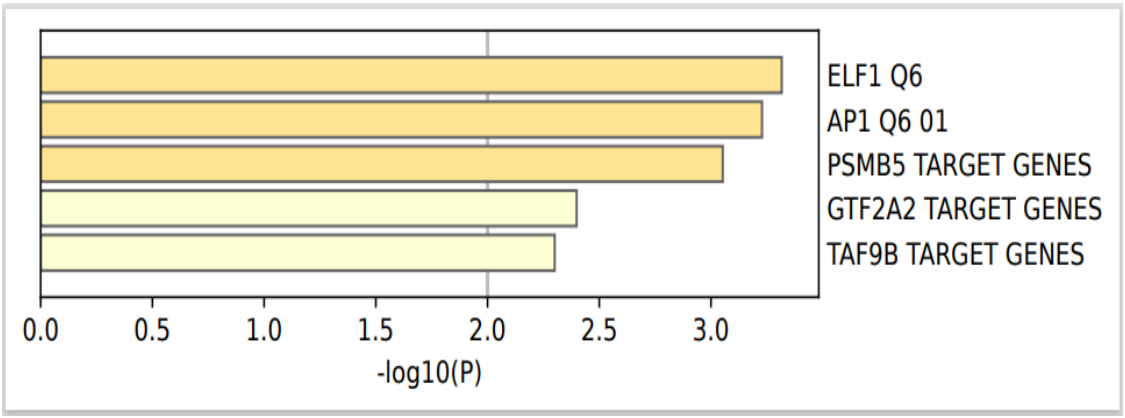

Fig. S21. **(A.)**) A protein–protein interaction (PPI) network was generated using representative genes from the identified cancer cell clusters via the GeneMANIA web server. **(B.)** Pathway enrichment analysis was performed using representative genes from the macrophage cell clusters through the MetaScape web server. (**C.**) Transcription factor enrichment analysis was conducted using representative genes from the cancer cell clusters.